Fabrication, Characterization, and Photoelectrocatalytic Application of ZnO Nanorods Grafted on Vertically Aligned TiO2 Nanotubes

ARTICLE *in* THE JOURNAL OF PHYSICAL CHEMISTRY C · OCTOBER 2009

Impact Factor: 4.77 · DOI: 10.1021/jp9071179

6 AUTHORS, INCLUDING:

Xili Tong
Chinese Academy of Sciences
36 PUBLICATIONS **387** CITATIONS

Fabrication, Characterization, and Photoelectrocatalytic Application of ZnO Nanorods Grafted on Vertically Aligned TiO_2 Nanotubes

Yanzhu Lei, Guohua Zhao,* Meichuan Liu, Zhongning Zhang, Xili Tong, and Tongcheng Cao

Department of Chemistry, Tongji University, Shanghai 200092, China

Received: July 26, 2009; Revised Manuscript Received: September 18, 2009

In this article, ZnO nanorods (NRs) were grafted on Ti-based vertically aligned TiO_2 nanotubes (NTs) by a feasible seed-induced hydrothermal reaction. Through such a simple but interesting structure combination of the two semiconductors, a novel composite photocatalytic anode of ZnO NRs/TiO_2 NTs with high efficiency was accordingly obtained. In this coupling, ZnO NRs could grow to flowerlike clusters directly grafted on the tops of TiO_2 NTs, acting just like a large number of lead wires, outstretched from the trunk TiO_2 NTs. Thus, the grafted ZnO NRs could serve conveniently as favorable hole channels and receptors for the efficient separation of photoelectrons and holes, which resulted in a slight shift of the band gap absorption edges and consequently changed the band gap energy (Eg). Moreover, the graft amount would further make a certain impact on the Eg. With an appropriate graft amount, ZnO NRs/TiO_2 NTs exhibited broader optical absorption range and higher photocatalytic activity than pure TiO_2 NTs or ZnO NRs did. Under the illumination of 365 nm UV light, the photoelectric conversion efficiency was enhanced from 7.0% of pure TiO_2 NTs to 23.6% of ZnO NRs/TiO_2 NTs. In the photoelectrocatalytic oxidation application, ZnO NRs/TiO_2 NTs exhibited higher removal ability for bisphenol A (BPA). The kinetic constant was 21.4×10^{-5} s^{-1}, almost 2.3 times faster than that on pure TiO_2 NTs. Also, the stability of ZnO NRs was promoted on TiO_2 NTs with a stable BPA cyclic removal percentage because the receipted holes on ZnO NRs could prevent ZnO from photocorrosion efficiently.

1. Introduction

By now, TiO_2 is known to be one of the most efficient and stable photocatalyst and has attracted more and more interests.[1−5] As another promising heterogeneous photocatalyst, ZnO is also an excellent n-type semiconductor with good photocatalytic (PC) activity. It is reported that, compared with TiO_2, ZnO exhibits comparable efficiency for the photoelectrocatalytic (PEC) oxidation of organic contamination.[6−8] However, because of the quick recombination rate of the photogenerated electron−hole pairs and the limited light responding range, the photoelectric conversion efficiencies of pure TiO_2 or ZnO are relatively low. It is also reported that ZnO even suffers the critical drawback of photocorrosion, which greatly reduces the photoactivity and photostability.[9,10] Therefore, these fundamental disadvantages have remained major obstacles in the practical application of TiO_2 or ZnO in PC degradation.

To solve this problem, significant efforts have been devoted to enhance the PC properties by manipulating the nanostructures or controlling the morphological of TiO_2 and ZnO,[3,11] coating with polymers,[12] and surface doping with other species,[12,13] such as nonmetallic elements, metal ions, and semiconductor oxides.[14−23] Among them, the nanosized coupling of TiO_2 and ZnO has attracted considerable interest to enhance photogenerated charge separation[24,25] because the formation of heterojunction structure shows some effects on the inhibition for the recombination of photogenerated electrons and holes and improves the stability. Although the band gap energies of ZnO and TiO_2 are similar to each other,[26,27] the potentials of the conduction band and the valence band of ZnO are charged a bit more negative. Thus, lower band gap energy may be obtained by the combination. The ZnO−TiO_2 composite nanoparticles (NPs),[24,25] nanofilms,[28−30] and other hybrids[31−38] with different nanostructures and a more stable state have been synthesized successfully. Researches have proved that the utilization of the nanocrystalline TiO_2 coupled with nanosized ZnO could improve their PC efficiency due to the synergistic effect on PC properties. However, in the form of disordered powder, the ZnO−TiO_2 composite suffers from the problem of recycling.[8,38] When coupled as nanofilms, the stability is too low to well realize the PEC application in electric field.

In view of this fact, the structure design of composite ZnO−TiO_2 is important to enhance the PEC activities and stability. This goal is of great interest to be achieved by a reasonable combination of ordered structure and appropriate control of the composite ratio. It is noticed that vertically aligned and highly ordered TiO_2 NTs prepared by anodic oxidation on Ti[3,39−41] not only exhibit higher PC efficiency than ordinary random TiO_2 nanoparticles and commercial Degassu P-25[41,42] but also show good physical and chemical stability, providing high specific surface area. The high cation-exchange character as well as the particular open mesoporous morphology and more free space make it easier for the bond of other photocatalysts on the nozzles of TiO_2 NTs.[43,44] All of these interesting properties of 1D TiO_2 NTs make it a promising support material for loading different photocatalysts. Meanwhile, with the ease and successful preparation on a variety of substrates, the vertical 1D ZnO NRs array has attracted more and more concern in the field of PC application.[45,46] Compared with nanoparticles and nanofilms, 1D ZnO NRs are ordered and vertically aligned on the substrates. The formation of specific hexagonal-shaped crystal will promote the PC activity to a large extent, which can be used for the PC degradation of aromatic pollutions in

* To whom correspondence should be addressed. E-mail: g.zhao@mail.tongji.edu.cn.

10.1021/jp9071179 CCC: $40.75
Published on Web 10/08/2009

wastewater, such as chlorophenol and methyl orange.[34,45] When the two 1D ordered nanostructures are coupled in a suitable way with a controllable structure and appropriate amount, higher surface area and more active sites are expected to be obtained. They may exhibit simultaneously high synergic PC activity and special physical chemistry properties.

On the bases of these discussions, it is proposed to fabricate novel vertically grafted 1D ZnO NRs on the tops of TiO_2 NTs. The key technology is to obtain such a graft with high efficiency and stability by a structure controllable method. Compared with nanoparticles or nanofilms, this graft 1D−1D structure is undoubtedly more controllable and ordered. Unlike disordered composites, which are in the form of packing or mixing, ZnO NRs and TiO_2 NTs are coupled by point junction. Such a noble composite manner may ensure the full exposure of TiO_2 NTs and sustain the morphology and properties of ZnO NRs, the PC effect of TiO_2 NTs and ZnO NRs can exert simultaneously. More importantly, a better separation of the electron−hole pairs may be achieved in this composite catalyst, and the stability of ZnO NRs is also expected to be improved. However, the impacts of the 1D−1D composite structure and the graft amount on the PC performance are rarely reported.

In this work, a new attempt has therefore been made to construct 1D−1D structured ZnO−TiO_2 photocatalyst. The photoelectric conversion efficiency and the stability were further investigated. By using the facile seed-induced hydrothermal synthesis route, ZnO NRs were grafted on vertically aligned TiO_2 NTs. The morphology, structure, and optical properties were characterized by SEM, XRD, UV−vis diffuse reflection, and Raman spectrum, respectively. The photoelectric activity of this composite structured catalyst was evaluated in detail by linear sweep voltammetry, and the photoelectric conversion efficiency was compared with pure TiO_2 NTs. The mechanism for enhancement of photoelectrocatalysis on ZnO NRs/TiO_2 NTs composite electrode was proposed. On the basis of these experiments, the impact of the graft amount and morphology of ZnO NRs on the PC activity was investigated. Bisphenol A (BPA), which was widely used in the manufacture of polycarbonate, epoxy resin, and numerous plastic articles, was selected as the target pollutant in our work because it was also demonstrated to be an endocrine disruptor with environmental harmfulness.[47,48] The enhancement in PEC degradation of BPA at ZnO NRs/TiO_2 NTs with a different graft amount is compared from removal percentage and kinetic parameter. To evaluate the inhibition of photocorrosion, the stability of the grafted ZnO NRs on TiO_2 NTs was also investigated by cyclic degradations of BPA. This article provides a feasible and facile method to combine ZnO NRs with vertically aligned TiO_2 NTs by point junction. The novel 1 D ZnO NRs/TiO_2 NTs PC anode with high efficiency and stability is promising in environmental application.

2. Experimental Methods

2.1. Reagents and Apparatus. Pure titanium foils (99.9% purity) cut into 1.5 × 4.0 cm^2 pieces were used for anodic oxidation. Zinc nitrate hydrate (Zn $(NO_3)_2$) and hexamethylenetetramine ($(CH_2)_6N_4$) were of analytical grade and used without further purification. All of the other reagents were of analytical grade. Double-distilled water was used throughout the experiments.

Field emission scanning electron microscope (EFEG-SEM, Model Quanta 200 FEG, FEI) and X-ray diffraction (XRD) (Bruker Co., Ltd., Germany) were used to characterize the morphology and crystal structure of the as-prepared electrodes. The optical absorption characteristics of the electrode are determined by UV−vis diffuse reflectance spectroscopy (UV−vis DRS, Model BWS002, manufacturers BWtek). The surface contact angles were measured with a sessile drop contact angle meter (JC2000A, Zhongchen) at room temperature and ambient humidity. A sessile drop of water (about 5 μL) was placed carefully onto the as-prepared electrode using a manual microsyringe fixture.

2.2. In Situ Growth of Ordered Vertically Aligned TiO_2 NTs on Ti Substrate. TiO_2 NTs based on Ti substrate were fabricated by anodic oxidation.[22,44] Briefly, titanium foil of 0.80 mm thickness was used as the substrate electrode. Prior to anodization, the titanium foils were mechanically polished with different emery papers to a mirrorlike finish. Then they were ultrasonically cleaned in distilled water and acetone for 20 min, respectively. After being rinsed thoroughly with double-distilled water, the clean titanium foil electrode was first etched in an 18 wt % HCl solution at 85 °C for 10 min. The etched titanium foil was rinsed thoroughly with double-distilled water and then anodized using a two-electrode system with an interelectrode gap of 1 cm. Titanium foil was used as the anode, and platinum foil was used as the counter electrode at the applied voltage of 20 V. The electrolyte consisted of 0.5 wt % NaF, 2 wt % Na_2SO_4, and 10 wt % polyglycol (400). After 3 h, TiO_2 NTs arrays formed on the Ti substrate. Finally, the as-prepared TiO_2 NTs were annealed at 500 °C under oxygen ambience for 5 h with heating and cooling rate of 1 °C /min to obtain stable NTs.

2.3. Graft of ZnO NRs on TiO_2 NTs. First of all, a layer of ZnO seeds was coated on the surface of TiO_2 NTs substrate using the sol−gel method. Briefly, ZnO coating precursor solution was prepared, in which 5 mM $Zn(CH_3COO)_2$ was dissolved in ethanol with stirring at 60 °C for 0.5 h to yield a homogeneous solution. Subsequently, the precursor solution was dropped on the clean substrate, spun at 100 rpm for 3 s, and then spun at 3000 rpm for 10 s. This procedure was repeated for 10 times. Then the substrate was dried in air and heated to 350 at 2 °C min^{-1} and held at 350 °C for 0.5 h to obtain a dense and uniform distribution of a ZnO seed layer on the substrate. Then hydrothermal synthesis of ZnO NRs followed. The growing precursor solution for chemical bath deposition was prepared by dissolving equal molar Zn $(NO_3)_2$ and $(CH_2)_6N_4$ in deionized water to form 0.02 mol L^{-1} (zinc and amine concentration) solutions. Then the substrates were suspended in the precursor solutions upside down in a Teflon-lined stainless steel autoclave at 90 °C for a certain time. Subsequently, the resultant films were washed with deionized water to remove any residual materials and dried at room temperature. To measure the graft amount (θ) of ZnO NRs on TiO_2 NTs, EDTA complexometric titration was used.

2.4. Measurement of the Photoelectric Catalysis of ZnO NRs/TiO_2 NTs. The photocurrent density was measured in 0.1 M Na_2SO_4 solution. A 15 W UV lamp (center wavelength 254 nm, light intensity 2 mW cm^{-2}) and a 300 W UV lamp (center wavelength 365 nm, light intensity 22 mW cm^{-2}) were used as the UV light sources. Photoelectric conversion efficiency at a certain bias voltage could be calculated in accordance with the following formula:[49]

$$\eta(\%) = [(\text{total power output} - \text{electrical power input})/\text{light power input}] \times 100 = j_p(E_{rev} - |E_{app}|) \times 100/I_0$$

where j_p is the photocurrent density (mA cm^{-2}), j_pE_{rev} is the total power output, j_pE_{app} is the electrical power input, and I_0 is the power density of the incident light (mW cm^{-2}). E_{rev} is the

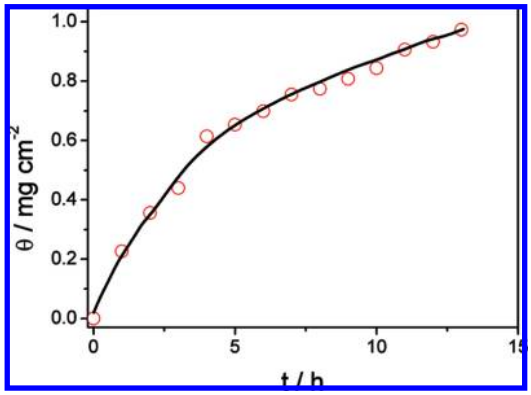

Figure 1. Graft amount of ZnO NRs with different hydrothermal times on TiO_2 NTs.

standard reversible potential (which is 1.23 V for the water splitting reaction at pH = 0), and E_{app} is the absolute value of the applied potential, which is obtained as $E_{app} = E_{means} - E_{ocp}$, where E_{meas} is the electrode potential of the working electrode at which j_p was measured under illumination and E_{ocp} is the applied potential at open circuit in the same electrolyte and under the same illumination.

Photoelectrochemical properties were measured in the standard three-electrode system on a CHI660C electrochemical workstation (CHI Co.), with the ZnO NRs/TiO_2 NTs electrode as the working electrode, platinum fossil as the counter electrode, and saturated calomel electrode (SCE) as the reference electrode. The surface area of the working electrode was 4.5 cm^2. The sweep potential range was −0.5 to 1.2 V, with the scan rate of 50 mV/s.

2.5. PEC Oxidation of BPA. PEC degradation experiment was carried out in a 100 mL quartz electrolytic cell. The cell was cooled with recycled water to maintain the temperature of the reaction system at 25 °C. ZnO NRs/TiO_2 NTs electrode served as the PC anode, titanium as cathode. They were placed in parallel in the reactor with a separation of 1.0 cm. The electrode area was 4.5 cm^2. The applied cell potential was 3.6 V (approximately 2.0 V vs SCE). A 300 W UV lamp was used as the light source, providing a light intensity of 3 mW cm^{-2}. Twenty-five mg L^{-1} BPA solution was prepared in 0.05 mol L^{-1} Na_2SO_4 solution, and the processing volume was 100 mL.

At a certain period of time, 1 mL sample was collected for chromatography determination. The concentration of BPA was tested by HPLC (Varian 3900 HPLC) with a phenyl column (4.6 × 150 mm, 5 μm) at 25 °C. The mobile phase was 50% water: 50% methanol and the flow rate was 1.0 mL min^{-1}. The detection wavelength was 230 nm. Samples were filtered by 13 mm × 0.20 mm micropore filter before injecting.

The degradation of BPA solutions was characterized by the removal of their total organic carbon (TOC), measured on a Shimadzu TOC-Vcpn analyzer.

3. Results and Discussion

3.1. Graft and Characterization of ZnO NRs on In Situ-Prepared Vertically Aligned TiO_2 NTs. The seed-induced hydrothermal process is used to graft ZnO NRs on the nozzles of TiO_2 NTs. These ZnO seeds have been demonstrated to be beneficial to the growth of ZnO NRs.[50] We've found that the graft amount can be conveniently manipulated by simply varying the hydrothermal time. Figure 1 shows the relationship between the graft amount and the hydrothermal time. It is observed that the graft amount of ZnO NRs increased from 0.23 to 0.65 mg cm^{-2} sharply with the hydrothermal synthesis time increases from 1 to 5 h. After 5 h, the increase of the graft amount slows down. When the hydrothermal time reaches 13 h, ZnO NRs cover the whole TiO_2 NTs with a graft amount of 0.98 mg cm^{-2}.

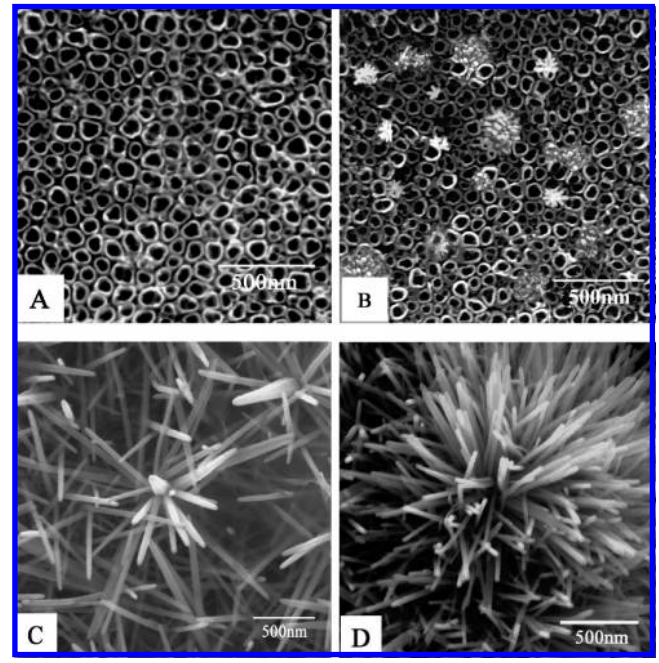

Figure 2. SEM image of as-prepared TiO_2 NTs (A) and ZnO NRs/TiO_2 NTs with different graft amount: (B) 0.23, (C) 0.65, (D) 0.98 mg cm^{-2}.

SEM images that show morphologies of pure TiO_2 NTs and ZnO NRs/TiO_2 NTs with the graft amount of 0.23, 0.65, and 0.98 mg cm^{-2} are displayed in Figure 2. Pure TiO_2 NTs on Ti substrate are highly ordered and compactly arranged (part A of Figure 2). The tubes are uniform in length and vertically align with the diameter of 50 to 90 nm. The thickness of the tube wall is from 10 to 15 nm. The gap between the tubes is around 20 nm. Part B of Figure 2 shows that ZnO NRs are mainly graft with the center of the seed, and some cover the nozzles of the tubes when small amounts (0.23 mg cm^{-2}) are grafted on the tops of TiO_2 NTs. When the graft amount increases to 0.65 mg cm^{-2} (hydrothermal time 5 h), abundant 1D ZnO NRs are grafted on the NTs (part C of Figure 2). They are in the form of irregular six-prism with the diameters of 50 nm and the lengths of about 1 μm. The flowerlike clusters act just like numerous lead wire, outstretched from the trunk TiO_2 NTs, which loom under these NRs. Furthermore, when the graft amount increases to 0.98 mg cm^{-2} (part D of Figure 2), the surface of the electrode is completely covered with ZnO NRs clusters. The diameter of these nanorods is still 50 nm but the length increases to 1.5−2 μm. The NRs grow very close with very narrow interplanar spacing. In some regions, the NRs even overlap, forming dense ZnO layer.

The XRD patterns of the ZnO NRs/TiO_2 NTs with different graft amount are shown in part A of Figure 3. Curve a obviously displays that the TiO_2 NTs demonstrate a regular anatase crystal structure, for the appearance of characteristic diffraction peaks at 25.3°, 37.9°, 48.2°, 53.8°, and 55.0°, corresponding to the (101), (004), (200), (105), and (211) facets. In addition, the diffraction peak at 27.5° corresponding to the rutile crystal phase can also be observed, indicating that TiO_2 NTs exhibit a composite crystalline form with anatase and rutile phases. In curves b to d, ZnO NRs/TiO_2 NTs exhibits not only characteristic anatase diffraction peaks of TiO_2 but also other new

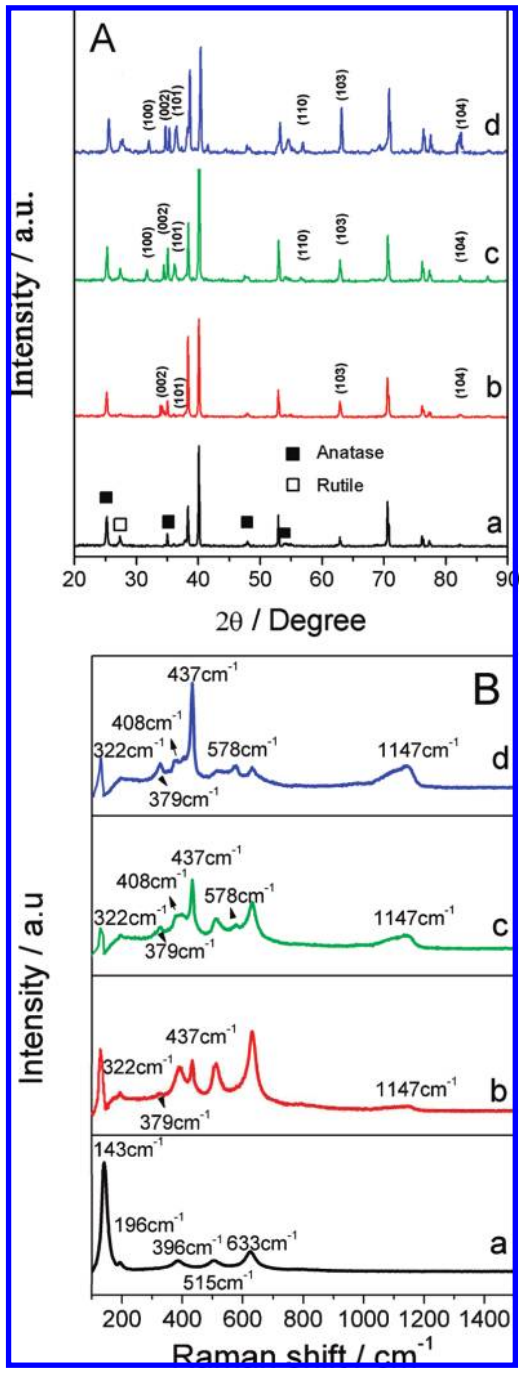

Figure 3. (A) XRD patterns of (a) TiO2 NTs and ZnO NRs /TiO_2 NTs samples with the graft mass of (b) 0.23, (c) 0.65, and (d) 0.98 mg·cm^{-2}. (B) Raman patterns of (a) TiO_2 NTs and ZnO NRs /TiO_2 NTs samples with the graft mass of (b) 0.23, (c) 0.65, and (d) 0.98 mg cm^{-2}.

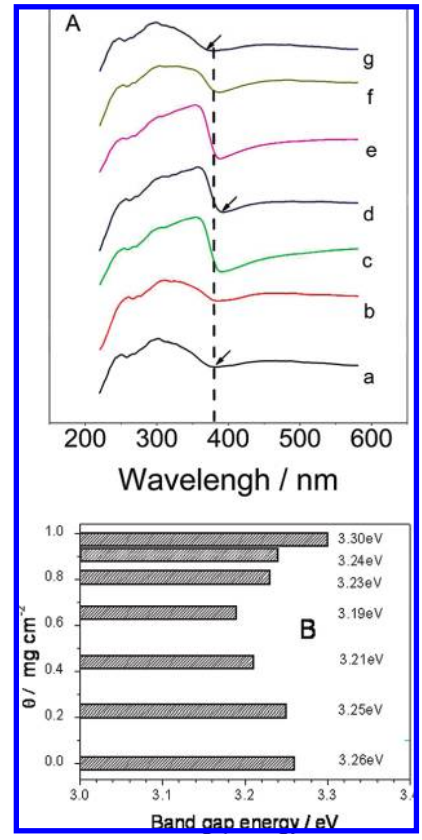

Figure 4. (A) UV−vis DRS spectrum of TiO_2 NTs and ZnO NRs/TiO_2 NTs with different graft amount. (B) Gap energy of ZnO NRs/TiO_2 NTs samples with different graft amount. (a) 0, (b) 0.23, (c) 0.44, (d) 0.65, (e) 0.77, (f) 0.81, and (g) 0.98 mg cm^{-2}.

diffraction peaks at 31.9°, 34.6°, 36.4°, 56.6°, 62.9°, and 83.5°, corresponding to (100), (002), (101), (110), (103), and (104) facets of ZnO. All of the diffraction peaks can be exactly indexed as the hexagonal wurtzite ZnO, which is in good agreement with the values in the standard card (JCPDS 36−1451). As the grafted amount of ZnO NRs increases, the intensity of the diffraction peaks at 34.6°, 36.4°, 62.9°, and 83.5° also increase, ascribed to the ZnO (002), (101), (103), and (104) crystal facets. When the graft amount is 0.65 mg cm^{-2} (part A of Figure 3, curve c), in addition to (002), (101), and (103) crystal facets, the diffraction peaks at 31.9° can also be observed for (100) crystal facets. As the graft amount increases to 0.98 mg cm^{-2} (part A of Figure 3, curve d), there is a diffraction peak that appears at 56.6° for the (110) crystal facet. When large amounts of ZnO NTs cover the whole surface of TiO_2 NTs, they even show the typical crystal facet peaks of pure ZnO.

The UV Raman scattering measurements are used to investigate the vibrational properties of the ZnO NRs/TiO_2 NTs, which can also be used to confirm the graft of ZnO on TiO_2 NTs (part B of Figure 3). As for TiO_2 NTs (part B of Figure 3, curve a), the remarkable peaks at 143, 396, 515, and 633 cm^{-1} are associated with the E_g, E_g, B_{1g}, A_{1g} anatase vibration modes of TiO_2, respectively. The weak peak located at 196 cm^{-1} corresponds to the E_g mode.[51] When ZnO NRs are successfully grafted on TiO_2 NTs, it can be seen that the peak at 143 cm^{-1} is unconspicuous. The remarkable E_{2H} mode of ZnO is located at 437 cm^{-1}, which corresponds to the characteristic band of the hexagonal wurtzite phase. The weaker peaks appearing at 379 and 415 cm^{-1} can be assigned to the A_1(TO) and E_1(TO) modes of ZnO, respectively. In addition, the appearance of the E_1(LO) mode at 578 cm^{-1}, which is associated with oxygen deficiency, indicates that ZnO NRs have a certain level of oxygen vacancies.[45] Obviously, the intensity of the peak at 437 cm^{-1} increases as the graft amount increases. It is also true for the peak at 1147 cm^{-1}, which attributed to multiphonon scattering processes.[27]

3.2. PEC Activity of ZnO NRs/TiO_2 NTs. Part A of Figure 4 shows the typical UV−vis diffuse reflection spectra (DRS) of pure TiO_2 NTs and ZnO NRs/TiO_2 NTs at room temperature, which indicate the band gap absorption edges of the composite electrodes. As shown in part A of Figure 4, curve a, in the UV light region, TiO_2 NTs present a continuous wide absorption

SCHEME 1: Schematic Illustration of the Band Gap Energy and Charge Separation of the Combined ZnO NRs/TiO_2 NTs under UV Light Irradiation

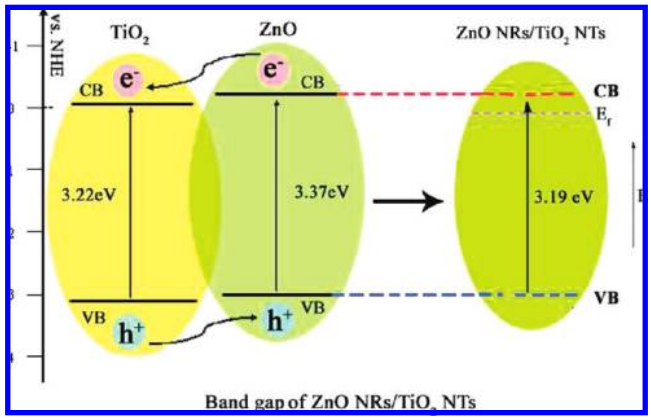

band. The maximum absorption peak locates at around 300 nm. The band gap absorption edge is around 380 nm. According to the formula Eg = 1240/λ,[52] the band gap energy (Eg) can be calculated to be 3.26 eV. Part A of Figure 4, curves b to g, display the DRS spectrum of ZnO NRs/TiO_2 NTs with different graft amounts. When a certain amount of ZnO NRs are grafted, obvious changes of the adsorption peak shapes could be observed. In the UV region, from 320 to 375 nm, the continuous UV absorption band is wider than that of TiO_2 NTs. Upon increasing of the graft amount of ZnO NRs from 0 to 0.65 mg cm^{-2}, the maximum peaks red shift to around 370 nm. In the λ > 375 nm region, a red shift of the band gap absorption edge can also be observed. When the graft amount increases to 0.65 mg cm^{-2}, the band gap absorption edge shifts to 388.6 nm, indicating that the Eg is 3.19 eV. However, further increasing the graft amount of ZnO NRs brings a bit of a blue shift of the maximum adsorption peak and the band gap absorption edge. When ZnO NRs almost cover the whole surface of TiO_2 NTs (Ca. 0.98 mg cm^{-2}), the maximum peak in the UV region shifts back to 300 nm. While in the λ > 375 nm region, the band gap absorption edge shifts to 376.0 nm, indicating the Eg is 3.30 eV, even higher than pure TiO_2 NTs. Part B of Figure 4 shows the corresponding relationship between Eg and the graft amount. Obviously, as the graft amount increases, the Eg first decreases and then increases gradually. The lowest point is 3.19 eV, corresponding to the graft amount of 0.65 mg cm^{-2}, and the wholly covered ZnO NRs/TiO_2 NTs shows the highest Eg of 3.30 eV.

The red shift of band gap absorption edge and the change of the Eg can be explained by the band gap theory. Scheme 1 shows the mechanism of the separation of electron−hole pairs. As illustrated in this scheme, although the band gap energies of ZnO and TiO_2 are similar,[26,27] the potentials of the conduction band and the valence band of ZnO charged a bit more negative. When ZnO combines with TiO_2 to form complex semiconductor photocatalyst, upon band gap excitation, as it is more sensitive, ZnO is excited first, and electron−hole pairs are generated. In terms of energetics, the photogenerated electrons inject into the conduction band of TiO_2 NTs from that of the excited ZnO NRs, which correspondingly changes the bottom of the conduction band, decreasing the band gap of the ZnO NRs. Thereon, it is favorable for the TiO_2 to be more excited. On the other hand, the transfer of photogenerated hole also occurs from the valence band of TiO_2 NTs to that of ZnO NRs, causing an oxidation reaction. Hence, there would be more electrons transferring to TiO_2 NTs, causing reduction reaction with O_2 at the surface. Thus, the interfacial electron transfer from ZnO to TiO_2 can effectively separate the electrons and holes, inhibiting the recombination of electron−hole pairs.

Furthermore, compared with traditional disordered ZnO/TiO_2 composites, ordered 1 D ZnO NRs/TiO_2 NTs also shows comparatively high PC activity. However, unlike the disordered form, ordered ZnO NRs/TiO_2 NTs can be directly used as an anode for the PEC application in the electric field, even under a high applied potential. It can be explained by the following assumption. As is known, the combine of ZnO NRs and TiO_2 NTs leads to the elevation of the Fermi level of the composite ZnO NRs/TiO_2 NTs, which is near the conduction band. Meanwhile, in the electric field, when the applied potential is more positive than the flat-band potential, it promotes the electrons' transfer from the electrolyte to the ZnO NRs/TiO_2 NTs, resulting in an increase of band bending. More importantly, the 1D flowerlike clusters of ZnO NRs act like a large number of lead wires, which are directly outstretched from the trunk TiO_2 NTs. They are speculated to be convenient for the transfer of holes from trunk TiO_2 NTs to the ZnO NRs. Such an efficient charge separation will decrease the recombination of electron−hole pairs and accordingly increase the lifetime of the charge carriers. Thus, the coupling of the two semiconductors in a suitable ratio and the applying of a proper potential will result in more efficient interfacial charge separation and transfer to adsorbed substrates. This mechanism is in accordance with literatures.[53,54] However, from Figure 4, it is also assumed that the graft amount will affect the Eg in some degree. Thus, with an appropriate graft amount, ZnO NRs/TiO_2 NTs electrode may exhibit a higher photoelectric performance.

The photoelectric performance and PEC efficiency of the ZnO NRs/TiO_2 NTs are further investigated by linear-sweep photovoltammetry. It is known that TiO_2 NTs exhibit excellent UV absorption and PC activity under short-wave UV light. Thus, the photoelectric responses of TiO_2 NTs and ZnO NRs/TiO_2 NTs are studied by using a 254 nm irradiation. As shown in part A of Figure 5, the rise of the photocurrent corresponds well with the illumination of a UV light of 254 nm. First, the current response on both pure TiO_2 NTs and ZnO NRs/TiO_2 NTs in dark is even at a potential of up to 2.0 V, which means that no electrochemical oxidation occurred. However, under the illumination of 254 nm UV light, a significant increase in the photocurrent is observed. It increases as the applied potential is scanned toward more positive potential, indicating that the photogenerated electrons can be effectively driven by positive potential. The photocurrent density of pure TiO_2 NTs is 0.32 mA cm^{-2}. When the graft amount of ZnO NRs is 0.65 mg cm^{-2}, the photocurrent reaches the maximum value (0.92 mA cm^{-2}), about 3 times higher than that on pure TiO_2 NTs. Since then, as the graft amount increases, the photogenerated current density gradually decreases. When the surface is wholly covered with ZnO NRs (0.98 mg cm^{-2}), the photocurrent density decreases to 0.35 mA cm^{-2}, similar to that of pure TiO_2 NTs. The results well demonstrate that an elevated photocurrent density is obtained on the ZnO NRs/TiO_2 NTs with proper graft amount for its higher light response in UV light region. Apart from the enhancement of light absorption, the grafted ZnO NRs also contribute to the photocurrent produced because they could facilitate the charge separation.

The above results are further proved by the data of photoelectric conversion efficiency (η). On the basis of Formula 1, η of different electrode can be calculated. As shown in part B of Figure 5, under 254 nm UV light, the $\eta_{254\ nm}$ first increases with the graft amount increasing. With a graft amount of 0.65 mg

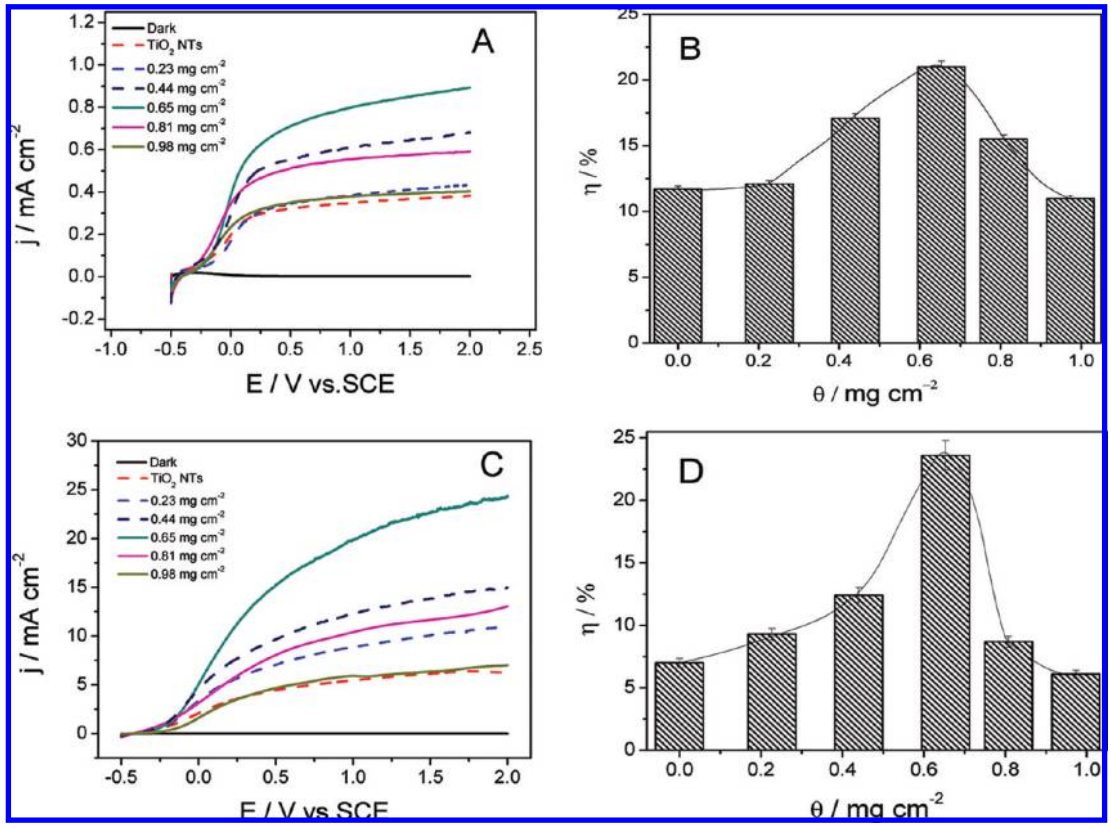

Figure 5. (A) Linear-sweep photovoltammograms of TiO_2 NTs and ZnO NRs/TiO_2 NTs with different graft amounts under the illumination of 254 nm UV light. (B) Photoelectric conversion efficiency of ZnO NRs/TiO_2 NTs with different graft amount under 254 nm UV light. (C) Linear-sweep photovoltammograms of TiO_2 NTs and ZnO NRs/TiO_2 NTs with different graft amounts under the illumination of 365 nm UV light. (D) Photoelectric conversion efficiency of ZnO NRs/TiO_2 NTs with different graft amount under 365 nm UV light. Photovoltammograms were all obtained at 50 mV/s.

cm^{-2}, the $\eta_{254\ nm}$ is about 21%, whereas on TiO_2 NTs, it is only 11.7%. Thus, the modification of TiO_2 NTs by a proper graft of ZnO can promote the η under the illumination of 254 nm UV light.

Moreover, as displayed in the UV−vis DRS spectrum, it is noticed that the graft structure of ZnO NRs on TiO_2 NTs results in a slight red shift of the absorption edges. Thus, we consider that the composite ZnO NRs/TiO_2 NTs might exhibit higher photoelectric activity under a longer wave UV light. On the basis of this, investigation under the irradiation of 365 nm wavelength UV light is carried out. The photocurrent density increases with the graft amount of ZnO NRs, and with the graft amount of 0.65 mg cm^{-2}, the photocurrent density is the largest (around 23 mA cm^{-2}), over 4 times higher than that on pure TiO_2 NTs (part C of Figure 5). The $\eta_{365\ nm}$ is calculated to be 23.6%, whereas for TiO_2 NTs it is 7.0% (part D of Figure 5).

To compare these PEC results with PC properties of ZnO NRs/TiO_2 NTs, the η of the electrode at the open circuit potential (OCPT) can also be studied. The photogenerated current density at the OCPT was recorded under the illumination of UV light. According to formula 1, with the graft amount of 0.65 mg cm^{-2}, the η_{OCPT} is 3.2% and 20.4% under 254 nm and 365 nm wavelength UV light, respectively.

For a better comparison, the photoelectric efficiency of pure TiO_2 NTs and ZnO NRs/TiO_2 NTs are listed in Table 1. As for pure TiO_2 NTs, because of the easier electron−hole recombination, both η_{254} and η_{365} are relatively low at the OCPT (2.3% and 4.6%). Thus, the practical PC application of TiO_2 NTs is constrained. However, when a certain degree of bias potential is applied, the photoelectric conversion efficiency increases to

TABLE 1: Comparison of the PEC Activities of ZnO NRs/TiO_2 NTs and pure TiO_2 NTs

	TiO_2 NTs	ZnO NRs/TiO_2 NTs	
Eg (eV)		3.26	3.19
$\eta_{254\ nm}$ (%)	PC	2.3	3.2
	PEC	11.7	21.0
	increment	9.4	17.8
$\eta_{365\ nm}$ (%)	PC	4.6	16.4
	PEC	7.0	23.6
	increment	2.4	7.2

11.7% and 7.0% respectively indicating a higher η_{254} can be obtained in electric field than η_{365}. Therefore, in the practical application of pure TiO_2 NTs, a 254 nm UV light is usually selected, and also a certain bias potential is applied to promote the electron−hole separation.

Contrarily, once appropriate ZnO NRs (0.65 mg cm^{-2}) are grafted on TiO_2 NTs, both η_{254} and η_{365} at OCPT are highly increased, much higher than that of pure TiO_2 NTs. It is remarkable that, under the irradiation of 365 nm UV light, η_{365} is still of a relatively high value (16.4%) even though no bias potential is applied. This phenomenon may ascribe to an obvious red shift of the light absorption on ZnO NRs/TiO_2 NTs with an appropriate graft amount. Thus, this composite photocatalyst can extend the light absorption spectrum and improve the absorption efficiency for the long-wave light. The practical application of this ZnO NRs/TiO_2 NTs electrode may be extended to 365 nm or a longer wave range. When certain bias potential is applied, the enhancement of η is more pronounced under both 254 and 365 nm UV light. The increments ($\eta_{PEC}-\eta_{PE}$) are 17.8% and 7.2% for 254 and 365 nm respec-

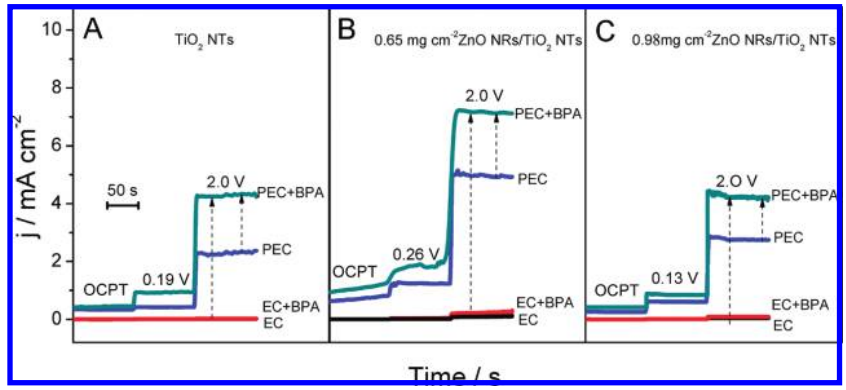

Figure 6. Variation of photoelectric oxidation current density when different bias potential is applied for the degradation of BPA on TiO_2 NTs (A), 0.65 mg cm^{-2} ZnO NRs/TiO_2 NTs (B), and 0.98 mg cm^{-2} ZnO NRs/TiO_2 NTs (C).

tively, much higher than that of pure TiO_2 NTs (11.4% and 2.7%, respectively). This may be due to the effect of ZnO NRs on the efficient separation of the electrons and holes.

Thus, it can be concluded that, besides the effect of formed heterojunction, the graft structure, and appropriate graft amount of ZnO NRs also play important roles in the PC properties of the ZnO NRs/TiO_2 NTs electrode. First, the impact of the structure on the PEC performance can be assumed as follows. For the pure TiO_2 NTs, the photogenerate electrons and holes can be only separated on TiO_2 NTs themselves. The electron−hole pairs easily recombine, reducing the PC efficiency. As for pure ZnO, it is found that the surface recombination occurs more easily. Hence, the charge carrier lifetime is much shorter.[55] However, when appropriate ZnO NRs are grafted, PC properties increase because the possibility of recombination between photogenerated electron and hole is reduced. In this conjunction, ZnO NRs serve in a manner as numerous channels, which are convenient for the rapid transfer of holes. Thus, the electrons and holes are separated efficiently.

Second, the graft amount also shows a significant effect on the enhancement of PEC activity. When the graft amount of ZnO NRs is relatively low, the effect of charge separation induced by ZnO NRs is not obvious because of the insufficiency of the channels. However, when ZnO NRs wholly cover the surface of TiO_2 NTs with a relatively large graft amount, a large number of active sites on TiO_2 NTs will be blocked. The contact between TiO_2 NTs and oxygen-contained species is also hindered, which might result in the decrease of PC properties. Contrarily, when the graft amount is appropriate, the property of TiO_2 NTs can be fully exposed and the morphology and properties of ZnO NRs can be sustained. They provide adequate channels that can promote the rapid transfer of the holes. Therefore, the grafted ZnO NRs on TiO_2 NTs not only lower the band gap energy from 3.26 to 3.19 eV, resulting in the red shift of the band absorption edge, which is more conducive to the long-wavelength UV absorption, but also further reduce the recombination of the electron−hole pairs efficiently.

3.3. PEC Oxidation of BPA. The investigation of the PC oxidation for BPA on ZnO NRs/TiO_2 NTs electrode is further carried out compared with pure TiO_2 NTs. The structure of BPA is as follows:

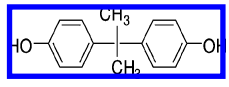

First of all, the PC and PEC oxidation current density comparison during the photoelectrolysis of BPA under different bias potentials is investigated. Three potentials are applied for this study, namely at the OCPT, at a potential where the PC anode exhibits the highest photoelectric conversion efficiency and at a higher bias potential of 2.0 V versus SCE, respectively. As shown in part A of Figure 6, on pure TiO_2 NTs, nearly no obvious oxidation current can be observed in dark after the injection of BPA. However, under the illumination of 365 nm UV light, the oxidation current density increase to 0.55, 1.02, and 4.98 mA cm^{-2} at the OCPT, 0.19 and 2.0 V versus SCE, respectively. On ZnO NRs/TiO_2 NTs with a graft amount of

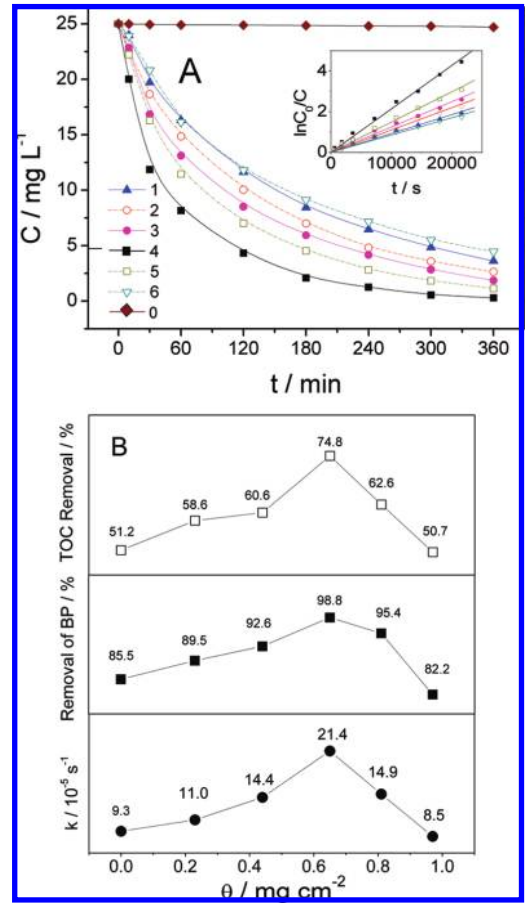

Figure 7. (A) Photolysis (0) and PEC removal of BPA on TiO_2 NTs (1) and on ZnO NRs/TiO_2 NTs with different graft amount: (1) 0, (2) 0.23, (3) 0.44, (4) 0.65, (5) 0.81, and (6) 0.98 mg cm^{-2}; insert: The relationship between the natural logarithm concentration of BPA and the time. (B) Calculated k, concentration removal percentage and TOC removal percentage of BPA on ZnO NRs/TiO_2 NTs with different graft amounts.

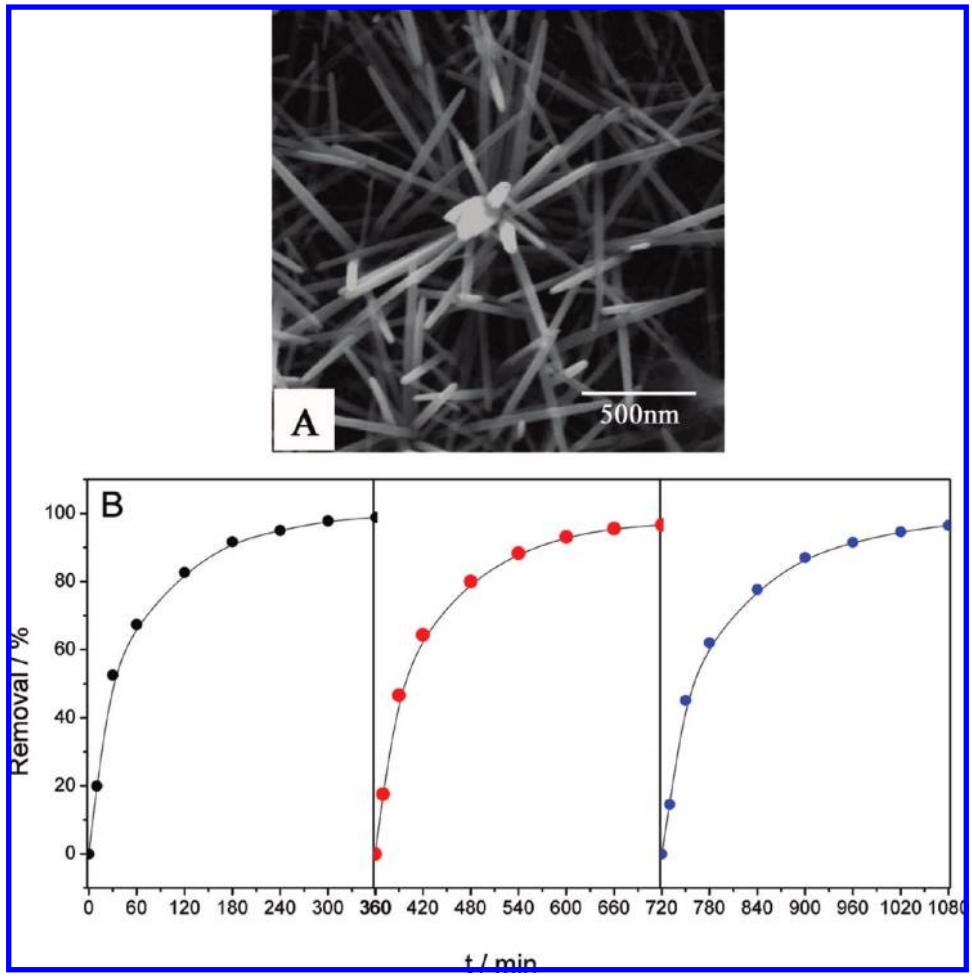

Figure 8. (A) SEM image of ZnO NRs/TiO_2 NTs (0.65 mg cm^{-2}) after 6 h degradation; (B) removal percentage of BPA after 6 h with cyclic photoelectric degradation.

0.65 mg cm^{-2} (part B of Figure 6), at the OCPT, there is also no obvious oxidation current in dark after the injection of BPA under the illumination of 365 nm UV light, and the photo current density increases to 0.93 mA cm^{-2}. At the potential at which the highest photoelectric conversion efficiency is obtained (ca. 0.26 V vs SCE), it increases to 2.1 mA cm^{-2}. When a bias potential of 2.0 V versus SCE is applied, it increased to 7.1 mA cm^{-2}. Similarly, the change of PC oxidation current density of BPA on ZnO NRs/TiO2 NTs (0.98 mg cm^{-2}, fully covered by ZnO NRs; part C of Figure 6) indicates that under the applied potential of 2.0 V, the PEC oxidation current density (4.92 mA cm^{-2}) is higher than that at the OCPT (0.61 mA cm^{-2}) and 0.13 V versus SCE (1.21 mA cm^{-2}). Therefore, the potential of 2.0 V versus SCE is considered to be appropriate and applied for the PEC degradation of BPA.

Part A of Figure 7 shows the photolysis and PEC degradation of BPA on pure TiO_2 NTs and ZnO NRs/TiO_2 NTs with different graft amounts. Without applying any photocatalyst, BPA removal is only 1.2% even after 6 h by UV photolysis. Thus, only photolysis is not efficient for the degradation of BPA. During the PEC oxidation process, it is found that the removal percentage of BPA increases with the graft amount of ZnO NRs changing from 0 to 0.65 mg cm^{-2}. Afterward, the removal percentage decreased when the graft amount is higher than 0.65 mg cm^{-2}. This law of change is in accordance with the above investigation on the PEC activity. On pure TiO_2 NTs, the BPA and TOC removal percentages are 85.5% and 51.2% after 6 h degradation respectively, with a relevant lower rate constant (k) of 9.3 $\times$ 10^{-5} s^{-1}. As is the case on ZnO NRs/TiO_2 NTs with appropriate graft amount (0.65 mg cm^{-2}), during the first 1 h process the BPA concentration decreased sharply. Only after 30 min, the BPA removal reaches to more than 50%. This may be ascribed to the fast cleavage of the carbon chain in the middle of the two benzene rings during the initial time. However, the removal rate slows down after 1 h degradation. That is because the cleavage of the benzene ring on the electrode is in such a slow manner. After 6 h degradation, the removal of BPA is 98.8%, and the TOC removal is 74.8%. The k of BPA degradation on ZnO NRs/TiO_2 NTs can be calculated to be 2.14 $\times$ 10^{-4} s^{-1}, indicating that a faster degradation process can be obtained on this electrode than that on pure TiO_2 NTs. As is the case on ZnO NRs/TiO_2 NTs with overabundant graft amount of ZnO NRs, the removal percentages of BPA and TOC are 82.2% and 50.7% respectively, and the k is 8.5 $\times$ 10^{-5} s^{-1}, even lower than that on pure TiO_2 NTs. It may be attributed to the whole coverage of ZnO NRs on TiO_2 NTs, which block the exertion of the PC activates of both ZnO and TiO2 NTs. Therefore, ZnO NRs/TiO_2 NTs anode with appropriate graft amount shows the highest PEC performance. When compared with commercial Degassu P-25 TiO_2,[56,57] the dosage of several hundred milligrams should be applied in the solution or spread on the substrates, and, after several hours, the BPA removal could reach to more than 80%. However, in this study, the graft amount of ZnO NRs is only 0.65 mg cm^{-2}. Thus, if only 2.925 mg P-25 (with the equal qulity of ZnO NRs on TiO_2 NTs) was added into BPA solution with an initial concentration of 25 mg

L^{-1}, the BPA removal by PC oxidation could not be higher than 5% even after 6 h. The results indicate that ZnO NRs/TiO_2 NTs exhibits high PEC activity than the PC activity of P-25 for the degradation of BPA. On the other hand, the applied potential further promotes the charge separation, resulting in a higher PEC activity.

It is known that ZnO photocatalyst suffers from photocorrosion in practical application;[10,54,58] thus, it is of great importance to study the stability of ZnO NRs/TiO_2 NTs during the PEC degradation. The morphology and structure of ZnO NRs/TiO_2 NTs electrode after the whole process was investigated by SEM and XRD. The SEM image of ZnO NRs/TiO_2 NTs (0.65 mg cm^{-1}) was taken after 6 h degradation. As shown in part A of Figure 8, the grafted ZnO NRs can still be observed without any distinct change of the morphology. From XRD patterns (not given), it can be found that the crystalline phase structure of ZnO NRs/TiO_2 NTs electrode after 6 h degradation is similar to the as-prepared ZnO NRs/TiO_2 NTs. To further evaluate the PEC stability, recycled experiments for the degradation of BPA were performed. As shown in part B of Figure 8 98.8% of BPA could be removed within 6 h for the first time. After three recycles, 96.5% of BPA could still be removed by ZnO NRs/TiO_2 NTs (0.65 mg cm^{-2}) within 6 h. These results indicate that by a facile combination, the photocorrosion of ZnO can be inhibited. The stability of the grafted ZnO NRs on TiO_2 NTs is accordingly enhanced. As is known, by using heterojunction structure, such as coupling with C_{60},[59] graphite-like carbon,[60] or other metals and semiconductors,[12,61−63] the stability of ZnO could be improved. Unlike these heterojunction structures, in which other particles, films, and polymer membranes serve as coating to protect the nanosized ZnO, the ZnO NRs/TiO_2 NTs 1D−1D graft structure is a point junction structure. ZnO NRs are fully exposed, which exhibits different photoelectric conversion mechanism, compared with ordinary ZnO. As several hole channels and suitable hole receptors, ZnO NRs make photogenerated holes transfer conveniently. ZnO is accordingly protected. By such a facile coupling method, ZnO NRs can also be protected against photocorrosion. This resolution is novel and feasible, providing a simple way to construct semiconductor composite catalysts with higher efficiency and stability.

4. Conclusions

In this article, a novel ZnO NRs grafted TiO_2 NTs composite photoelectrocatalyst was prepared to enhance the PEC activity. ZnO NRs was grafted on the vertically aligned NTs by a simple seed-induced hydrothermal process and the graft amount could be easily manipulated by controlling the hydrothermal time. Compared with pure TiO_2 NTs and disordered ZnO−TiO_2, the resultant ZnO NRs/TiO_2 NTs composite anode exhibited higher photoelectrocatalysis and stability. In this composite semiconductor PC system, ZnO NRs serve as excellent channels outstretched directly from TiO_2 NTs for the holes, which can efficiently promote the electron−hole separation and the charge transfer rate under a certain applied potential, resulting in the red shift of the band absorption edge. The light adsorption spectrum was accordingly extended and the photoelectric performance of the composite anode is further enhanced. The photocurrent density is found to be much higher on ZnO NRs/TiO2 NTs with a proper graft amount than that on TiO_2 NTs and the photoelectric conversion efficiency increased both under 254 and 365 nm irradiation. Experimental results showed that ZnO NRs/TiO_2 NTs with the graft amount of 0.65 mg cm^{-2} was the most effective anode for the fastest photoelectric degradation of BPA with the rate constant of 21.4×10^{-5} s^{-1}, almost 2.3 times higher than that on pure TiO_2 NTs. The stability of the grafted ZnO NRs was further enhanced because as hole receptors, the photocorrosion of ZnO NRs was inhibited efficiently. A primary insight into the structure−effect relationship of this novel composite semiconductor photocatalyst has been gained and a promising platform for fabricating the efficient PC anode has been accordingly provided.

Acknowledgment. This work was supported jointly by the National Natural Science Foundation of China (Project Nos. 20877058 and 20707015), 863 Program (Project No. 2008AA06Z329) from the Ministry of Science, and Nanometer Science Foundation of Shanghai (Project No. 0852 nm01200).

References and Notes

(1) Tian, M.; Adams, B.; Wen, J. L.; Asmussen, R. M.; Chen, A. C. *Electrochim. Acta* **2009**, *54*, 3799–3805.
(2) Wu, X. M.; Ling, Y. H.; Liu, L.; Huang, Z. H. *J. Electrochem. Soc.* **2009**, *156*, K65–K71.
(3) Liu, Z.; Zhang, X.; Nishimoto, S.; Jin, M.; Tryk, D. A.; Murakami, T.; Fujishima, A. *J. Phys. Chem. C* **2008**, *112*, 253–259.
(4) Lu, N.; Quan, X.; Li, J. Y.; Chen, S.; Yu, H. T.; Chen, G. H. *J. Phys. Chem. C* **2007**, *111*, 11836–11842.
(5) Macak, J. M.; Tsuchiya, H.; Ghicov, A.; Yasuda, K.; Hahn, R.; Bauer, S.; Schmuki, P. *Curr. Opin. Solid State Mat. Sci.* **2007**, *11*, 3–18.
(6) Khodja, A. A.; Sehili, T.; Pilichowski, J.-F.; Boule, P. *J. Photochem. Photobiol., A* **2001**, *141*, 231–239.
(7) Lizama, C.; Freer, J.; Baeza, J.; Mansilla, H. D. *Catal. Today* **2002**, *76*, 235–246.
(8) Kansal, S. K.; Singh, M.; Sud, D. *J. Hazard. Mater.* **2008**, *153*, 412–417.
(9) de Jongh, P. E.; Meulenkamp, E. A.; Vanmaekelbergh, D.; Kelly, J. J. *J. Phys. Chem. B* **2000**, *104*, 7686–7693.
(10) Hoffmann, M. R.; Martin, S. T.; Choi, W. Y.; Bahnemann, D. W. *Chem. Rev.* **1995**, *95*, 69–96.
(11) Jiang, Y. H.; Wu, M.; Wu, X. J.; Sun, Y. M.; Yin, H. B. *Mater. Lett.* **2009**, *63*, 275–278.
(12) Zhang, H.; Zong, R. L.; Zhu, Y. F. *J. Phys. Chem. C* **2009**, *113*, 4605–4611.
(13) Qiu, X. Q.; Li, L. P.; Zheng, J.; Liu, J. J.; Sun, X. F.; Li, G. S. *J. Phys. Chem. C* **2008**, *112*, 12242–12248.
(14) Zheng, L. R.; Zheng, Y. H.; Chen, C. Q.; Zhan, Y. Y.; Lin, X. Y.; Zheng, Q.; Wei, K. M.; Zhu, J. F. *Inorg. Chem.* **2009**, *48*, 1819–1825.
(15) Wang, H. H.; Baek, S.; Lee, J.; Lim, S. *Chem. Eng. J.* **2009**, *146*, 355–361.
(16) Wang, X. T.; He, Z.; Zhong, S. H. *J. Inorg. Mater.* **2009**, *24*, 215–220.
(17) Kontos, A. I.; Likodimos, V.; Stergiopoulos, T.; Tsoukleris, D. S.; Falaras, P.; Rabias, I.; Papavassiliou, G.; Kim, D.; Kunze, J.; Schmuki, P. *Chem. Mater.* **2009**, *21*, 662–672.
(18) Mohapatra, S. K.; Banerjee, S.; Misra, M. *Nanotechnology* **2008**, *19*, 315601–15608.
(19) Park, J. H.; Park, O. O.; Kim, S. *Appl. Phys. Lett.* **2006**, *89*, 3.
(20) Kuang, S. Y.; Yang, L. X.; Luo, S. L.; Cai, Q. Y. *Appl. Surf. Sci.* **2009**, *255*, 7385–7388.
(21) Izumi, Y.; Itoi, T.; Peng, S.; Oka, K.; Shibata, Y. *J. Phys. Chem. C* **2009**, *113*, 6706–6718.
(22) Li, P. Q.; Zhao, G. H.; Cui, X.; Zhang, Y. G.; Tang, Y. T. *J. Phys. Chem. C* **2009**, *113*, 2375–2383.
(23) Kim, J. C.; Choi, J.; Lee, Y. B.; Hong, J. H.; Lee, J. I.; Yang, J. W.; Lee, W. I.; Hur, N. H. *Chem. Commun.* **2006**, 5024–5026.
(24) Kostedt, W. L.; Ismail, A. A.; Mazyck, D. W. *Ind. Eng. Chem. Res.* **2008**, *47*, 1483–1487.
(25) Liao, D. L.; Badour, C. A.; Liao, B. Q. *J. Photochem. Photobiol., A* **2008**, *194*, 11–19.
(26) Yu, H. D.; Zhang, Z. P.; Han, M. Y.; Hao, X. T.; Zhu, F. R. *J. Am. Chem. Soc.* **2005**, *127*, 2378–2379.
(27) Yu, Q. J.; Fu, W. Y.; Yu, C. L.; Yang, H. B.; Wei, R. H.; Li, M. H.; Liu, S. K.; Sui, Y. M.; Liu, Z. L.; Yuan, M. X.; Zou, G. T.; Wang, G. R.; Shao, C. L.; Liu, Y. C. *J. Phys. Chem. C* **2007**, *111*, 17521–17526.
(28) Jiang, H. B.; Gao, L.; Zhang, Q. H. *J. Inorg. Mater.* **2003**, *18*, 695–699.
(29) Zhang, Z. H.; Yuan, Y.; Fang, Y. J.; Liang, L. H.; Ding, H. C.; Jin, L. T. *Talanta* **2007**, *73*, 523–528.
(30) Yang, S. G.; Quan, X.; Li, X. Y.; Liu, Y. Z.; Chen, S.; Chen, G. H. *Phys. Chem. Chem. Phys.* **2004**, *6*, 659–664.

(31) Wang, L. S.; Xiao, M. W.; Huang, X. J.; Wu, Y. D. *J. Hazard. Mater.* **2009**, *161*, 49–54.
(32) Wang, N.; Li, X. Y.; Wang, Y. X.; Hou, Y.; Zou, X. J.; Chen, G. H. *Mater. Lett.* **2008**, *62*, 3691–3693.
(33) Yang, Y.; Wang, X. H.; Sun, C. K.; Li, L. T. *J. Appl. Phys.* **2009**, *105*, 094304-1–94304-5.
(34) Zhang, Z. H.; Yuan, Y.; Liang, L. H.; Cheng, Y. X.; Shi, G. Y.; Jin, L. T. *J. Hazard. Mater.* **2008**, *158*, 517–522.
(35) Wang, Y. Q.; Sun, Y. M.; Li, K. *Mater. Lett.* **2009**, *63*, 1102–1104.
(36) Chen, D.; Zhang, H.; Hu, S.; Li, J. H. *J. Phys. Chem. C* **2008**, *112*, 117–122.
(37) Liu, G.; Li, G. S.; Qiu, X. Q.; Li, L. P. *J. Alloys Compd.* **2009**, *481*, 492–497.
(38) Zhang, Q.; Fan, W.; Gao, L. *Appl. Catal., B* **2007**, *76*, 168–173.
(39) Gong, D.; Grimes, C. A.; Varghese, O. K.; Hu, W. C.; Singh, R. S.; Chen, Z.; Dickey, E. C. *J. Mater. Res.* **2001**, *16*, 3331–3334.
(40) Mor, G. K.; Varghese, O. K.; Paulose, M.; Shankar, K.; Grimes, C. A. *Sol. Energy Mater. Sol. Cells* **2006**, *90*, 2011–2075.
(41) Paulose, M.; Shankar, K.; Yoriya, S.; Prakasam, H. E.; Varghese, O. K.; Mor, G. K.; Latempa, T. A.; Fitzgerald, A.; Grimes, C. A. *J. Phys. Chem. B* **2006**, *110*, 16179–16184.
(42) Liu, Z. Y.; Zhang, X. T.; Nishimoto, S.; Murakami, T.; Fujishima, A. *Environ. Sci. Technol.* **2008**, *42*, 8547–8551.
(43) Zhao, G. H.; Lei, Y. Z.; Zhang, Y. G.; Li, H. X.; Liu, M. C. *J. Phys. Chem. C* **2008**, *112*, 14786–14795.
(44) Zhao, G. H.; Cui, X.; Liu, M. C.; Li, P. Q.; Zhang, Y. G.; Cao, T. C.; Li, H. X.; Lei, Y. Z.; Liu, L.; Li, D. M. *Environ. Sci. Technol.* **2009**, *43*, 1480–1486.
(45) Wang, Y. X.; Li, X. Y.; Lu, G.; Quan, X.; Chen, G. H. *J. Phys. Chem. C* **2008**, *112*, 7332–7336.
(46) Wang, G.; Chen, D.; Zhang, H.; Zhang, J. Z.; Li, J. H. *J. Phys. Chem. C* **2008**, *112*, 8850–8855.
(47) Gozmen, B.; Oturan, M. A.; Oturan, N.; Erbatur, O. *Environ. Sci. Technol.* **2003**, *37*, 3716–3723.
(48) Murugananthan, M.; Yoshihara, S.; Rakuma, T.; Shirakashi, T. *J. Hazard. Mater.* **2008**, *154*, 213–220.
(49) Khan, S. U. M.; Al-Shahry, M.; Ingler, W. B. *Science* **2002**, *297*, 2243–2245.
(50) Greene, L. E.; Law, M.; Tan, D. H.; Montano, M.; Goldberger, J.; Somorjai, G.; Yang, P. D. *Nano Lett.* **2005**, *5*, 1231–1236.
(51) Yu, Y.; Yu, J. C.; Yu, J. G.; Kwok, Y. C.; Che, Y. K.; Zhao, J. C.; Ding, L.; Ge, W. K.; Wong, P. K. *Appl. Catal., A* **2005**, *289*, 186–196.
(52) Ji, P. F.; Zhang, J. L.; Chen, F.; Anpo, M. *J. Phys. Chem. C* **2008**, *112*, 17809–17813.
(53) Marci, G.; Augugliaro, V.; Lopez-Munoz, M. J.; Martin, C.; Palmisano, L.; Rives, V.; Schiavello, M.; Tilley, R. J. D.; Venezia, A. M. *J. Phys. Chem. B* **2001**, *105*, 1033–1040.
(54) Serpone, N.; Maruthamuthu, P.; Pichat, P.; Pelizzetti, E.; Hidaka, H. *J. Photochem. Photobiol., A* **1995**, *85*, 247–255.
(55) Kim, D. W.; Lee, S.; Jung, H. S.; Kim, J. Y.; Shin, H.; Hong, K. S. *Int. J. Hydrogen Energy* **2007**, *32*, 3137–3140.
(56) Wang, R. C.; Ren, D. J.; Xia, S. Q.; Zhang, Y. L.; Zhao, J. F. *J. Hazard. Mater.* **2009**, *169*, 926–932.
(57) Venkatachalam, N.; Palanichamy, M.; Arabindoo, B.; Murugesan, V. *Catal. Commun.* **2007**, *8*, 1088–1093.
(58) Spathis, P.; Poulios, I. *Corros. Sci.* **1995**, *37*, 673–680.
(59) Fu, H. B.; Xu, T. G.; Zhu, S. B.; Zhu, Y. F. *Environ. Sci. Technol.* **2008**, *42*, 8064–8069.
(60) Zhang, L. W.; Cheng, H. Y.; Zong, R. L.; Zhu, Y. F. *J. Phys. Chem. C* **2009**, *113*, 2368–2374.
(61) Wang, H. C.; Liu, P.; Wang, S. M.; Han, W.; Wang, X. X.; Fu, X. Z. *J. Mol. Catal., A* **2007**, *273*, 21–25.
(62) Stroyuk, A. L.; Shvalagin, V. V.; Kuchmii, S. Y. *J. Photochem. Photobiol., A* **2005**, *173*, 185–194.
(63) Comparelli, R.; Fanizza, E.; Curri, M. L.; Cozzi, P. D.; Mascolo, G.; Agostiano, A. *Appl. Catal., B* **2005**, *60*, 1–11.

JP9071179